Frantti, J.; Fujioka, Y.; Zhang, Jinsuo; Wang, S.; Vogel, Sven C.; Nieminen, Risto; Asiri, A. M.; Zhao, Y.; Obaid, A. Y.; Mkhalid, I. A.

High-pressure neutron study of the morphotropic lead-zirconate-titanate

Published in:
Journal of Applied Physics

DOI:
10.1063/1.4733570

Published: 01/07/2012

Document Version
Publisher's PDF, also known as Version of record

Please cite the original version:
Frantti, J., Fujioka, Y., Zhang, J., Wang, S., Vogel, S. C., Nieminen, R., Asiri, A. M., Zhao, Y., Obaid, A. Y., & Mkhalid, I. A. (2012). High-pressure neutron study of the morphotropic lead-zirconate-titanate: Phase transitions in a two-phase system. *Journal of Applied Physics*, *112*(1), 1-7. Article 014104.
https://doi.org/10.1063/1.4733570

High-pressure neutron study of the morphotropic lead-zirconate-titanate: Phase transitions in a two-phase system

J. Frantti' , Y. Fujioka, J. Zhang, S. Wang, S. C. Vogel, R. M. Nieminen, A. M. Asiri, Y. Zhao, A. Y. Obaid, and I. A. Mkhalid

Citation: Journal of Applied Physics **112**, 014104 (2012); doi: 10.1063/1.4733570
View online: http://dx.doi.org/10.1063/1.4733570
View Table of Contents: http://aip.scitation.org/toc/jap/112/1
Published by the American Institute of Physics

High-pressure neutron study of the morphotropic lead-zirconate-titanate: Phase transitions in a two-phase system

J. Frantti,[1,a)] Y. Fujioka,[1] J. Zhang,[2] S. Wang,[2] S. C. Vogel,[2] R. M. Nieminen,[1] A. M. Asiri,[3] Y. Zhao,[2] A. Y. Obaid,[3] and I. A. Mkhalid[3]
[1]*Department of Applied Physics, Aalto University School of Science, FI-00076 Aalto, Finland*
[2]*Los Alamos Neutron Science Center, Los Alamos National Laboratory, Los Alamos, New Mexico 87545, USA*
[3]*Chemistry Department, Faculty of Science, King Abdulaziz University, P.O. Box 80203, Jeddah 21589, Saudi Arabia and Center of Excellence for Advanced Materials Research, King Abdulaziz University, P.O. Box 80203, Jeddah 21589, Saudi Arabia*

(Received 30 January 2012; accepted 5 June 2012; published online 5 July 2012)

The present study was dedicated to the classical piezoelectric, lead-zirconate-titanate ceramic with composition $Pb(Zr_{0.54}Ti_{0.46})O_3$ at the Zr-rich side of the morphotropic phase boundary at which two phases co-exists. The pressure-induced changes in the phase fractions were studied by high-pressure neutron powder diffraction technique up to 3 GPa and 773 K. The two co-existing phases were rhombohedral $R3c$ and monoclinic Cm at room temperature and $R3c$ and $P4mm$ above 1 GPa and 400 K. The experiments show that pressure favors the $R3c$ phase over the Cm and $P4mm$ phases, whereas at elevated temperatures entropy favours the $P4mm$ phase. At 1 GPa pressure, the transition to the cubic $Pm\bar{3}m$ phase occurred at around 600 K. Pressure lowers the $Cm \rightarrow P4mm$ transition temperature. The Cm phase was found to continuously transform to the $P4mm$ phase with increasing pressure, which is inline with the usual notion that the hydrostatic pressure favours higher symmetry structures. At the same time, the phase fraction of the $R3c$ phase was increasing, implying discontinuous $Cm \rightarrow R3c$ phase transition. This is in clear contrast to the polarization rotation model according to which the Cm would link the tetragonal and rhombohedral phases by being a phase in which the polarization would, more or less continuously, rotate from the tetragonal polarization direction to the rhombohedral direction. Pressure induces large changes in phase fractions contributing to the extrinsic piezoelectricity. The changes are not entirely reversible, as was revealed by noting that after high-pressure experiments the amount of rhombohedral phase was larger than initially, suggesting that on the Zr-rich side of the phase boundary the monoclinic phase is metastable. An important contribution to the intrinsic piezoelectricity was revealed: a large displacement of the B cations (Zr and Ti) with respect to the oxygen anions is induced by pressure. © *2012 American Institute of Physics*. [http://dx.doi.org/10.1063/1.4733570]

I. INTRODUCTION

In piezoelectric ceramics, the changes in the phase stabilities versus stress and temperature in the vicinity of the phase boundary play a central role. Piezoelectric lead-zirconate-titanate [$Pb(Zr_xTi_{1-x})O_3$, PZT] solid solution system was developed over 40 years ago yet attempts to understand its properties continue to trigger new studies. A long-lasting view is that when x is approximately 0.52, a first-order phase transition occurs between tetragonal and rhombohedral phases, resulting in two-phase co-existence. The electromechanical properties peak slightly on the rhombohedral side of the phase boundary. In the composition-temperature plane, the boundary (commonly called as the morphotropic phase boundary, MPB) is nearly independent of temperature, thus making PZT very practical material for applications.[1] The commonly offered reasoning for the exceptionally good electromechanical coupling is based on the idea that there are eight (rhombohedral phase) and six (tetragonal phase) spontaneous polarization directions available in the two-phase system so that the system can readily respond to external electric field or stress.

The space group symmetries given for a disordered solid-solution should be taken as average symmetries from which short-range order deviates. For instance, it has been known for long that Raman scattering data cannot be explained by the average symmetries. The high-temperature cubic phase has no first-order Raman modes yet experiments revealed that spectra collected on PZT above the Curie temperature have rather strong features at energies close to the low-temperature first-order phonon energies. In the case of so-called relaxor ferroelectrics, this type of behavior is normal and the frequently offered explanation is that symmetry-lowering defects generate polar nanoregions (see, e.g., Refs. 2–4). Also, the low-temperature Raman spectra of Ti-rich PZT have many features which are not consistent with the tetragonal symmetry: the twofold degenerate E-symmetry modes of the tetragonal PZT were split, indicating that the symmetry is lower than $P4mm$.[5] Raman experiments showed that anharmonicity plays a significant role in lead titanate, the anharmonic contribution being increased with increasing temperature.[6] The traditional view was modified once high-resolution x-ray synchrotron

[a)]Electronic mail: johannes.frantti@aalto.fi.

studies revealed that the phase believed to be tetragonal possesses monoclinic distortion[7] in the vicinity of the MPB. Neutron powder diffraction experiments, able to resolve the monoclinic split,[8] ruled out octahedral tilts, and verified the *Cm* symmetry.[8,9]

Accurate modeling of the system requires not only the consideration of the unit cell but also crystallographic twins (or ferroelectric domains) and grain boundaries must be taken into account. In piezoelectric ceramics, the response to external stress or electric field can be divided into intrinsic and extrinsic contributions.[10] The former is essentially a single crystal response (i.e., is formed by the ion displacements within a primitive cell of the crystal), whereas the latter covers the contribution due to grain boundaries, preferred orientation or texture of the grains, i.e., ferroelectric domains within the grains, and changes in crystal phase fractions. Since the full model considering contributions from atomic scale up to the macroscopic grain size scale is very complex, experimental studies have commonly been applied to gain deeper insight.

Non-180° domain switching (i.e., contributing to the extrinsic contribution) gives rise to approximately 34% of the measured d_{33} coefficient of PZT.[11] The extrinsic contribution can be larger or smaller if the domain wall motion is, respectively, made easier or more difficult by doping.[12,13] A study of the domain switching showed that the 90° domains in single phase tetragonal phase (titanium rich PZT) hardly switch, whereas the domains in the two-phase region switch.[14] Texture and strain analysis of the ferroelastic behavior of $Pb(Zr_{0.49}Ti_{0.51})O_3$ by *in-situ* neutron diffraction technique showed that the rhombohedral phase plays a significant role in the macroscopic electromechanical behavior of this material.[15] The domain nucleation and domain wall propagation are central factors limiting the speed of ferroelectric polarization switching.[16,17]

An important intrinsic contribution to the piezoelectricity is due to the increase of certain piezoelectric constants once the phase transition is approached. This increase was predicted to be significant in the vicinity of the pressure-induced phase transition in lead titanate.[18] The computations carried out for lead titanate further show that it is the competition between two factors which determines the morphotropic phase boundary.[19] The first is the oxygen octahedral tilting, favoring the rhombohedral *R*3*c* phase, and the second is the entropy, which in the vicinity of the morphotropic phase boundary favors the tetragonal phase above 130 K. If the two factors are in balance over a large temperature range, a steep phase boundary results in the pressure-temperature plane which is desirable for applications. The advantageous feature of the *R*3*c* phase is its ability to be compressed efficiently by tilting the oxygen octahedra, in contrast to the *P*4*mm*, *Cm*, and *R*3*m* symmetries prohibiting oxygen octahedral tilting.[20]

We briefly summarize the relationship between the structural parameters and polyhedral tilts and volumes, given in Ref. 22, of the *R*3*c* phase. We follow Ref. 23 and parametrize the asymmetric unit of the *R*3*c* phase as given in Table I.

There is one short and one long O-O octahedral edge length parallel to the hexagonal *ab*-plane, labeled as $l - \Delta l$ and $l + \Delta l$, respectively, (see also Fig. 1). Now, the octahedral tilt angle is given by $\tan\omega = 3^{1/2}4e$ and the polyhedral volume ratio V_A/V_B is equal to $6K^2\cos^2\omega - 1$, where K is given by equation, $a = 2Kl\cos\omega$.

TABLE I. The asymmetric unit of the *R*3*c* phase as defined in Ref. 23.

	x	y	z
Pb	0	0	$s+\frac{1}{4}$
Ti/Zr	0	0	t
O	$\frac{1}{6}-2e-2d$	$\frac{1}{3}-4d$	$\frac{1}{12}$

Hexagonal, rhombohedral, monoclinic, and tetragonal axes lengths are very different. For the structure refinement of the rhombohedral phase, we use the hexagonal axes setting as it is more convenient (for definitions, see Ref. 24). Metrically, the distances and bond lengths of the corresponding atom pairs in different phases are sufficiently close to each other so that for the ease of comparison so called pseudo-cubic lattice parameters can be used. The parallelepiped defined by the pseudo-cubic lattice parameters enclose one ABO_3 formula unit. The pseudocubic monoclinic lattice parameters $a_{M,pc}$, $b_{M,pc}$, and $c_{M,pc}$ corresponding to the monoclinic axes lengths a_M, b_M, and c_M are given by $a_{M,pc} = a_M/\sqrt{2}$, $b_{M,pc} = b_M/\sqrt{2}$, and $c_{M,pc} = c_M$. The *R*3*c* phase (two formula units per rhombohedral cell) is a subgroup of the *R*3*m* phase (one formula unit per rhombohedral cell). The loss of mirror plane symmetry elements *m* corresponds to the doubling of the hexagonal c_H lengths: $c_H = c_H(R3c) = 2c_H(R3m)$ (see Fig. 1(a)). The pseudo-cubic

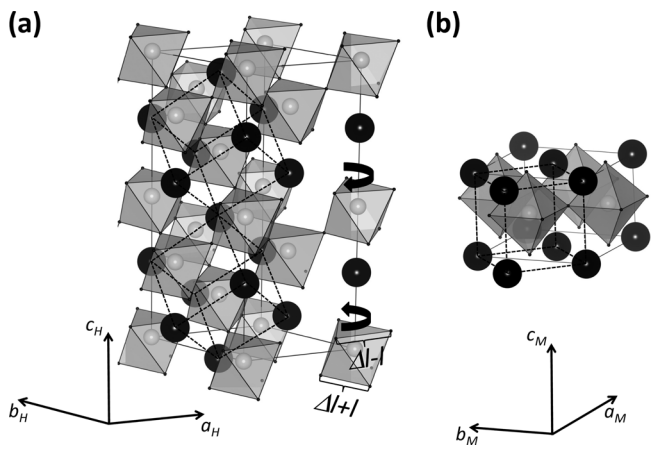

FIG. 1. The *R*3*c* phase, whose hexagonal unit cell is shown in panel (a), and the *Cm* phase, panel (b), behave very differently under applied pressure. The V_A/V_B ratio between the oxygen octahedral and cuboctahedra-volumes of the *R*3*c* phase decreases with increasing pressure: the crystal is contracting and thus the *B* cations (which fit oxygen octahedra tightly) have to take larger relative volume from the total volume (from the cuboctahedra, which has excess of space for Pb) by tilting oxygen octahedra. The symmetry prohibits this mechanism in the *P*4*mm* and *Cm* phases. Density-functional theory computations predict that *P*4*mm* has an entropy term benefit at elevated temperatures. Two rhombohedral (corresponding to the *R*3*m* phase) pseudocubic cells are shown by dotted lines in panel (a). Due to the octahedral tilting, indicated by arrows, the two cells are not equivalent: the tilting corresponds to the $R3m \rightarrow R3c$ symmetry lowering. The primitive cell of the *Cm* phase is shown by dotted lines in panel (b). Structure figure was prepared by the VESTA software.[21]

lattice parameters $a_{R,pc} = b_{R,pc} = c_{R,pc}$ of the $R3c$ phase are given in terms of the hexagonal axes a_H and c_H: $a_{R,pc} = \frac{1}{3}\sqrt{3a_H^2 + (c_H/2)^2}$. Below, we also give the angle $\alpha_R = 2\arcsin(3/(2\sqrt{3 + (c_H/a_H)^2}))$, which is the angle between any pair of the rhombohedral axes of the $R3c$ phase.

We are aware of one earlier high-pressure neutron powder diffraction work dedicated to MPB composition PZT, $Pb(Zr_{0.52}Ti_{0.48})O_3$, Ref. 25. However, the structural data reported in that study were not based on the two-phase model necessary for the MPB compositions, but instead the diffraction patterns were modeled by a single low-symmetry phase(s) in terms of a continuous polarization rotation. Thus, no estimates for the phase fractions were given in Ref. 25. There have been several attempts to model the co-existing phases, due to the first-order phase transition, by introducing a single low-symmetry phase in which the polarization would rotate continuously. This approach was discussed and disputed in Refs. 20 and 26. To extract meaningful structural data from a MPB region, a two-phase model is required. The present study focuses on the two-phase, Cm and $R3c$, PZT ceramic material, $Pb(Zr_{0.54}Ti_{0.46})O_3$, which has a composition slightly on the Zr-rich side of the MPB. The main goal was to determine the phase fractions and structural parameters as a function of applied pressure and temperature. Also, the question concerning the reversibility of the structural properties of PZT is addressed.

II. EXPERIMENTAL

To address the possible homogeneity differences due to the variation in solid-state reaction based sample preparation method lead zirconate-titanate powders were prepared using different starting oxides and sintering conditions. In the first route, the PbO, ZrO_2, and TiO_2 oxides were mechanically mixed in desired proportions, whereas in the second method $PbTiO_3$ and $PbZrO_3$ powders were used as starting chemicals. The phase purity and crystal structure were checked by x-ray powder diffraction (XRD) and scanning electron microscopy measurements. No significant differences were observed and thus a sample prepared through the former method was used for the experiments. Samples were annealed by first forming perovskite structure at 1073 K (30 min), then increasing the temperature to 1373 K (60 min) to improve the sample homogeneity and then cooling the sample in a stepwise manner to room temperature. Annealing times were kept rather short in order to limit PbO loss. XRD data were collected using CuK_α radiation at room temperature in Bragg-Brentano geometry. High-pressure neutron powder diffraction experiments were carried out at the Los Alamos Neutron Scattering Center using the TAP-98 toroidal anvil press[27,28] set on the high-pressure-preferred orientation (HIPPO) diffractometer.[29,30] Pressure was generated using the high-pressure anvil cells. Sodium chloride was used as a pressure calibrant material. To minimize deviatoric stress built up during room-temperature compression on the polycrystalline sample, all data in our high $P-T$ neutron-diffraction experiment were collected during the cooling cycle from 800 K at each desired loading pressure. Data were collected between 300 and 800 K as a function of pressure. Rietveld refinements were carried out using the programs General Structure Analysis System (GSAS)[31] and EXPGUI.[32] The pressure was estimated from the reflection positions of the NaCl phase through the equation of state.[33] The broad hump seen in the background intensity between 2 and 3 Å is due to the diffuse scattering from the amorphous zirconium phosphate gasket and was modeled using the diffuse scattering option available in the GSAS software.

III. RESULTS AND DISCUSSION

A. Structural model

The x-ray diffraction pattern collected on $Pb(Zr_{0.54}Ti_{0.46})O_3$ powder was characteristic to the morphotropic phase boundary composition, the most apparent indication of a two-phase co-existence is seen from the pseudo-cubic 200-reflections, see Fig. 2. Thus, the $R3c + Cm$ structural model (see Refs. 34, 36, and 37) was used for the refinements of the low-temperature data at ambient pressures. Fig. 2 shows also the room temperature neutron powder diffraction patterns measured at ambient pressure. Fig. 3 shows the

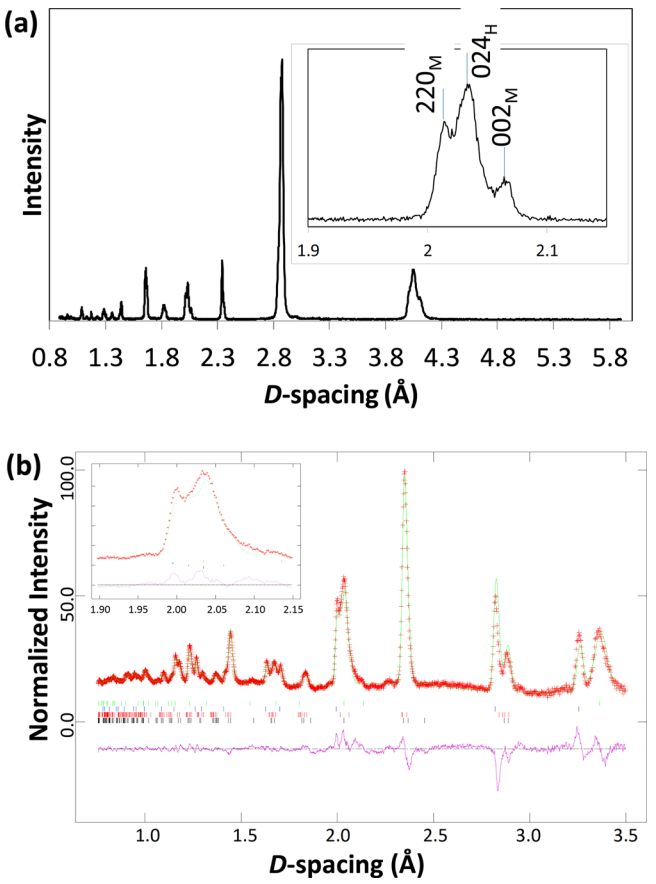

FIG. 2. (a) X-ray diffraction pattern measured from a $Pb(Zr_{0.54}Ti_{0.46})O_3$ sample at 303 K and 0 GPa, (b) observed (red) and calculated (green) time-of-flight neutron powder diffraction data and its difference curve between measured and computed curves (purple). The tick marks, from down to up, are from the $R3c$, Cm, NaCl (pressure standard), and graphite (from the pressure chamber) phases. Insets show the pseudo-cubic 200 reflections, labelled as 220_M and 002_M (Cm phase) and 024_H ($R3c$ phase). The lattice parameters were $a_M = 5.7207(14)$ Å, $b_M = 5.6785(14)$ Å, $c_M = 4.1211(10)$ Å and $\beta = 90.01(98)^\circ$ (Cm phase), and $a_H = 5.73533(59)$Å and $c_H = 14.2075(31)$Å ($R3c$ phase).

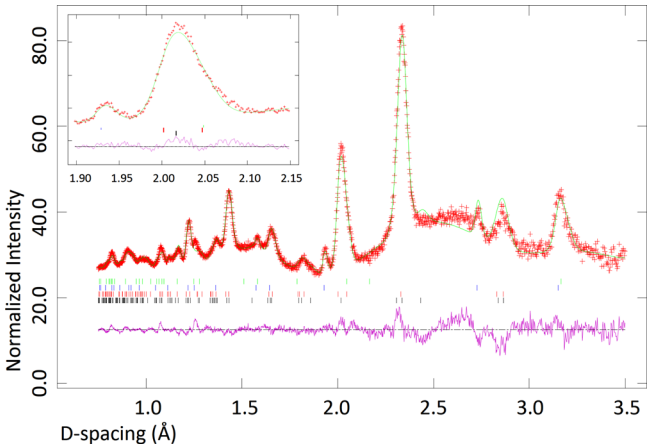

FIG. 3. Observed (red) and calculated (green) time-of-flight neutron powder diffraction data and its difference curve between measured and computed curves (purple) for a $Pb(Zr_{0.54}Ti_{0.46})O_3$ sample at 303 K and 3 GPa. The tick marks, from down to up, are from the *R*3*c*, *P*4*mm*, NaCl (pressure standard), and graphite (from the pressure chamber) phases. The inset shows the pseudo-cubic 200-reflection region (compare with Fig. 2).

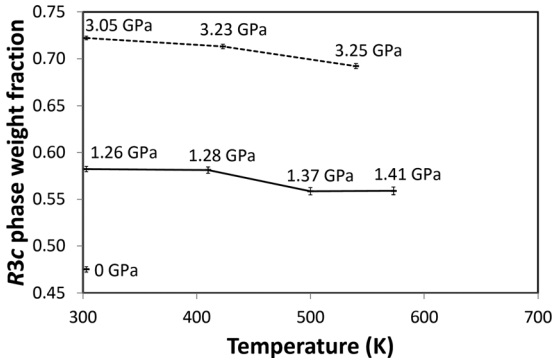

FIG. 4. Rhombohedral weight fraction at ambient conditions and as a function of temperature at approximately 1 and 3 GPa pressures.

pattern collected at 3 GPa pressure at room temperature and the intensity corresponding to the $P4mm + R3c$ phase model. Table II gives the statistical figures of merit for the refinements.

At ambient conditions, the majority phase was monoclinic, see the 0 GPa datum in Fig. 4. With increasing pressure the phase fractions changed significantly (Fig. 4), accompanied by large decrease in the lattice parameters of all phases (Fig. 5) and drastic changes in rhombohedral tilts and polyhedral volume fractions (Fig. 6). Slight decrease of the rhombohedral phase fraction with increasing temperature at constant pressure is seen in Fig. 4. This is in line with the ambient pressure behaviour, which revealed that the *Cm* phase fraction significantly increased and the monoclinic distortion decreased with increasing temperature.[34] Consistent findings were observed in synchrotron x-ray diffraction and first-principles calculation study on $Pb(Zr_{0.52}Ti_{0.48})O_3$, which revealed a phase transition sequence $Cm \rightarrow R3m \rightarrow R3c$ with increasing pressure at room temperature.[35] The first transition was reported to occur at around 2 and 3 GPa, whereas the latter took place between 6 and 7 GPa.

Refinements indicated that the monoclinic distortion continuously vanished with increasing hydrostatic pressure and increasing temperature. The monoclinic structure became tetragonal and was correspondingly modeled by the *P*4*mm* space group. Within a polarization rotation scheme the *Cm* phase is frequently assumed to be a bridging phase between the *P*4*mm* and *R*3*c* phases thus allowing continuous or weakly first-order phase transition sequence between the *P*4*mm* and *R*3*c* phases (such as $P4mm \rightarrow Cm \rightarrow R3c$ in simplest terms, though other variants are found in literature). However, the lattice parameters given in Fig. 5 indicate that the *Cm* phase does not continuously transform to the rhombohedral phase: the difference between the rhombohedral and monoclinic structures remains large up to the point (400 K, 1.3 GPa) at which the *Cm* phase continuously transforms to *P*4*mm* phase. At ambient pressure, the *Cm* phase was hardly distinguishable from the *P*4*mm* phase at 583 K.[34] These features are due to the fact that the *Cm* structure is derived from the *P*4*mm* structure by slightly displacing the ions along the ⟨110⟩ direction so that only one mirror plane is left. Hydrostatic pressure favours the higher symmetry phase. The $Cm \rightarrow P4mm$, $P4mm \rightarrow Pm\bar{3}m$, and $R3c \rightarrow Pm\bar{3}m$ transition temperatures are described by a line in $P - T$ plane. Though we do not have sufficient data to give pressure dependent phase transition temperatures in a form of a function, we note that all mentioned phase transition temperatures were decreasing with increasing pressure. The sample was cubic at 623 K at 1.3 GPa pressure. The structure was slightly distorted from a cubic structure at 573 K, so that the transition occurred between 573 and 623 K at 1.3 GPa.

Through the studied pressure and temperature range there are significant changes in the phase fractions. This is in line with the first-order phase transition and shows that no continuous polarization rotation occurs. Tilting the polarization direction would require very anisotropic external stimulus and it is our view, based on computational models[18–20] and the present experimental results, that such a symmetry lowering cannot be achieved by a high-symmetry external stimulus (e.g., hydrostatic pressure). Thus, the phase

TABLE II. Statistical figures-of-merit numbers as given by GSAS program. The χ^2 and *R* parameters are defined in the GSAS manual.[31] Reference to figures in which the refinement results were used is given. The results for different data sets are not always directly comparable as the data quality depends on the experimental conditions. For instance, at higher pressures the background contribution increases.

T(K)	*P*(GPa)	χ^2	R_{wp} (%)	R_p (%)	R_{bwp} (%)	R_{bp} (%)	Figures
303	1.26	2.433	2.89	1.94	3.73	2.26	4–7
410	1.26	2.085	2.92	1.96	3.86	2.37	4–7
500	1.37	2.212	3.00	2.05	4.17	2.53	4–7
573	1.41	2.212	3.01	2.09	4.12	2.62	4–7
623	1.47	1.195	4.15	2.92	8.13	4.16	4–7
773	1.81	1.221	4.19	2.96	7.20	4.30	4–7
303	0	5.643	4.00	2.75	7.10	3.69	2, 4, and 7
303	0	1.713	2.77	1.77	5.57	2.61	8
303	3.05	2.300	2.04	1.42	2.75	1.65	3–7
423	3.23	2.176	2.10	1.49	2.65	1.68	4–7
540	3.25	2.259	2.12	1.52	2.83	1.81	4–7
653	3.38	2.919	2.59	1.89	3.21	2.51	4–7
773	3.45	2.714	2.47	1.81	3.24	2.43	4–7

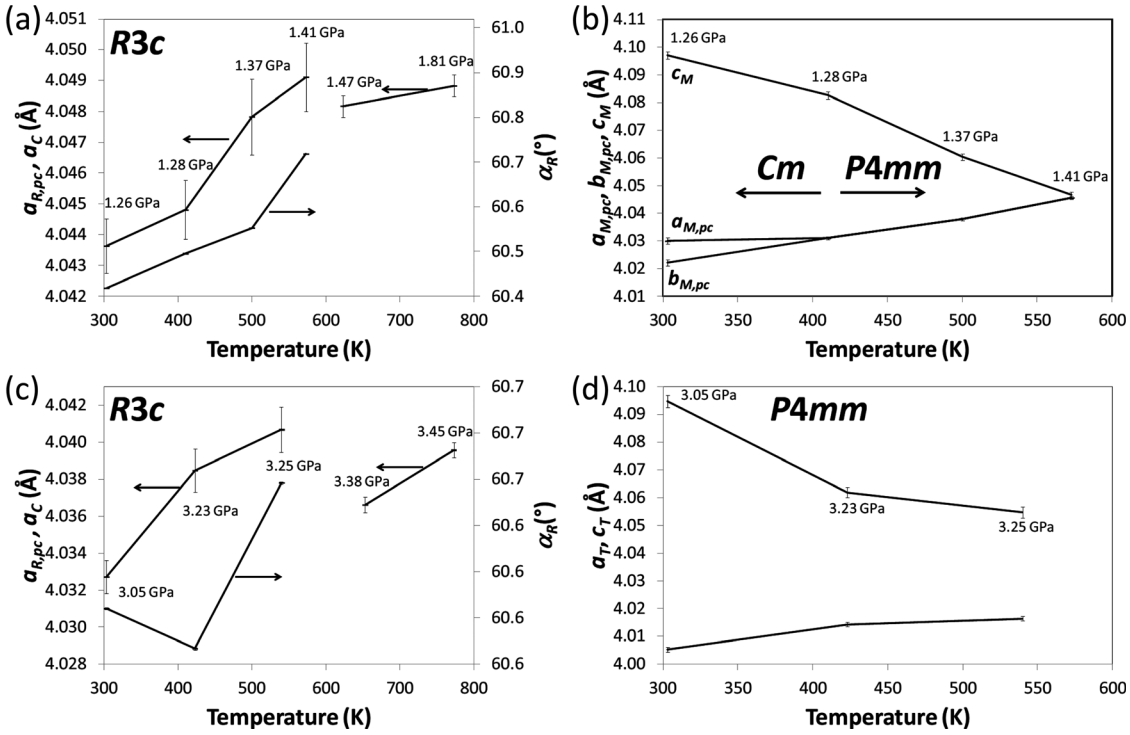

FIG. 5. Pseudo-cubic lattice parameters of the $R3c$, Cm, $P4mm$, and $Pm\bar{3}m$ phases as a function of temperature at approximately 1 GPa, panels (a) and (b), and 3 GPa pressures, panels (c) and (d). The Cm phase transformed to the $P4mm$ phase at around 400 K at 1 GPa pressure, panel (b). At 1.26 GPa pressure at room temperature the β angle was $90.62(4)^{\circ}$. The rhombohedral angle α_R is also given on right-hand side panels and is given with respect to the rhombohedral axes. Due to the thermal pressure, the pressure values of the highest two temperatures (cubic phase) are larger.

stabilities as a function of pressure and temperature follow well the predictions based on the first-principles studies carried out for $PbTiO_3$.[18,19] Further, the entropy term seems to have a crucial role for setting the boundary between the pseudo-tetragonal and rhombohedral phases: the pseudo-tetragonal phase fraction increases with increasing temperature at constant pressure.

B. Octahedral tilting

Figure 6 shows the octahedral tilts in the $R3c$ phase and the two characteristic octahedral edge lengths, $l - \Delta l$ and $l + \Delta l$. The octahedral tilt increases with increasing pressure, though the tilt angle saturates at high pressures. Thus with increasing pressure the volume fraction of the octahedra increases, consistently with the idea that, when compared to the tightly filled oxygen octahedra, lead ions have excessive space inside cuboctahedra formed from 12 oxygen atoms. In addition to the oxygen octahedral tilting also another mechanism can be seen: the continuous expansion of the $l + \Delta l$ and contraction of the $l - \Delta l$. Fig. 7(a) shows the B-cation (Zr or Ti) and oxygen bond lengths in the rhombohedral phase. At ambient conditions the B cations are closer to the larger oxygen triangle, consistently with the earlier data.[34] This situation changes with increasing pressure: it is seen that the B-cations are closer to the small oxygen triangle, indicating that at higher pressures the B-cations favour to form a small tetrahedron rather than being centered closer to the octahedron center, see the inset of Fig. 7. Positions in which the B cations are closer to the large triangle are clearly unfavourable as it would result in bond lengths failing to fullfill the bond-valence criteria. At 3 GPa pressure, the distance between the vertex of the large oxygen triangle and triangle center alone is slightly larger than the given B-O lengths. For piezoelectricity, this has important consequences: if stress is sufficiently strong, it switches the position of the B cations from a larger oxygen triangle towards the smaller oxygen triangle thus contributing to the intrinsic piezoelectricity. Thin film technology allows a deposition of selected crystal planes in which the biaxial stress can be adjusted by choosing the substrate and composition so that the piezoelectric properties can be optimized.

Fig. 7(b) gives the distance between the oxygen triangles, $D(l + \Delta l, l - \Delta l)$. Figs. 6(b) and 7(b) show that whereas $D(l + \Delta l, l - \Delta l)$ and $l - \Delta l$ both decrease and $l + \Delta l$ increases significantly when pressure increases from 0 to 1 GPa, $D(l + \Delta l, l - \Delta l)$ hardly changes when pressure increases from 1 GPa to 3 GPa. Instead, $l - \Delta l$ and $l + \Delta l$ decrease and increase significantly, respectively.

C. Reversibility

A first-order transition is frequently characterized by a two-phase co-existence region of metastable and stable phases as a function of the thermodynamic variable (e.g., temperature or pressure). In piezoelectric materials, this is one source of irreversibility (other significant contribution being due to the irreversible domain wall motion). It is interesting to note that the recovery run, carried out after the high-pressure and high-temperature cycles, revealed that the rhombohedral phase fraction had increased when compared to the prior the high-pressure situation, Fig. 8,

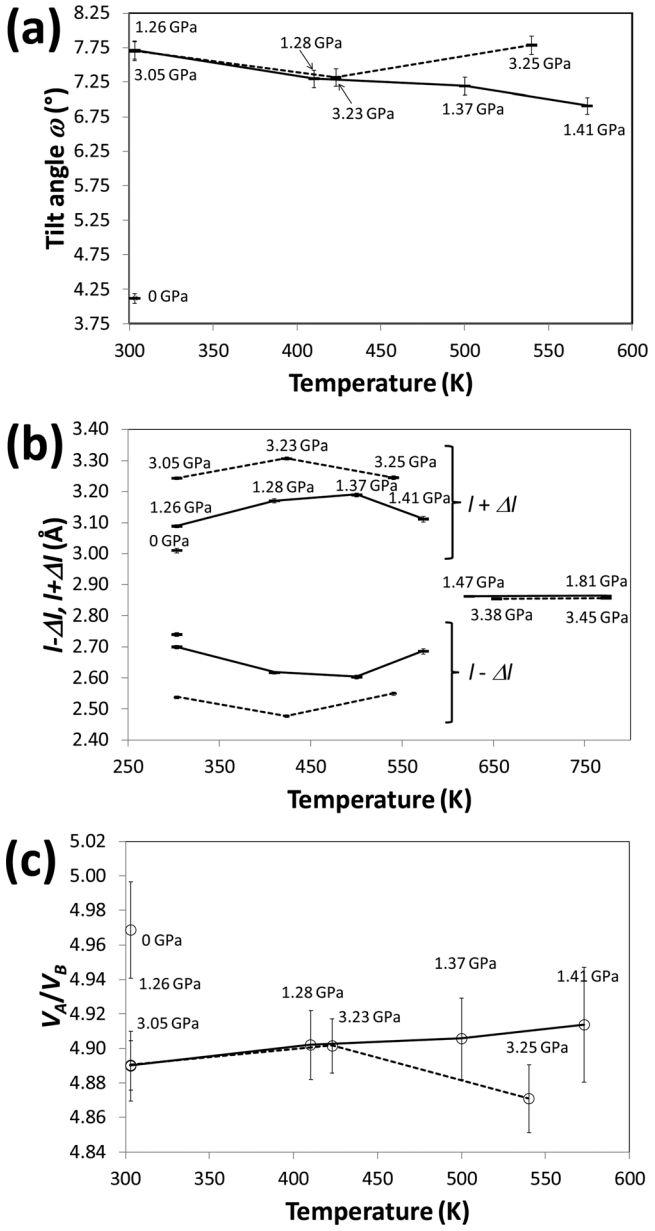

FIG. 6. Octahedral tilt angles (a), octahedral edge lengths (b), and polyhedral volume fractions of the $R3c$ phase at ambient conditions and as a function of temperature at approximately 1 and 3 GPa pressures.

being 0.633(4) (to be compared to the value 0.475(3) found in the sample before the high-pressure experiments). Latest and highest pressure applied on the sample before the recovery run was 5.6 GPa at room temperature. This suggests that high-pressure synthesis should be a useful way to prepare single-phase rhombohedral ceramics in the vicinity of the MPB. The advantage over the Zr-rich rhombohedral ceramics is that in the vicinity of the phase transition certain piezoelectric constants are more susceptible to external stimuli. We note that recent neutron powder[36] and single crystal[37] diffraction studies revealed that there is a secondary monoclinic Cm phase present in the Zr-rich case, together with the rhombohedral $R3m/R3c$ phases. Recent single crystal study also showed that the diffraction data, collected on $Pb(Zr_{0.54}Ti_{0.46})O_3$ and $Pb(Zr_{0.69}Ti_{0.31})O_3$ samples are better interpreted in terms of the rhombohedral and

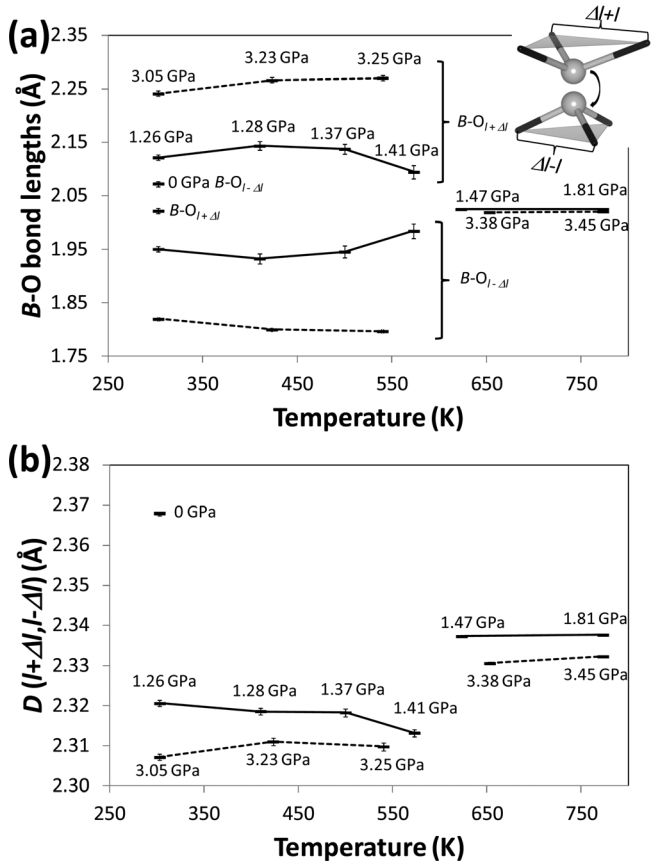

FIG. 7. (a) B-cation (Zr or Ti) and oxygen bond lengths in the rhombohedral phase. The difference between $B-O_{\Delta l+l}$ and $B-O_{\Delta l-l}$ bond lengths increases with increasing pressure. The decrease in difference seen at 1.41 GPa pressure is probably related to the vicinity of the transition to the cubic phase. (b) The distance $D(l+\Delta l, l-\Delta l)$ between the oxygen triangles. In both panels, the 3 GPa data are indicated by dotted lines. The inset shows the displacement of the B cations under pressure. At ambient pressures, the B is closer to the larger triangle and displaces towards smaller triangle under pressure.

monoclinic phases, rather than by the adaptive phase model.[38] The two-phase co-existence and the nature of the phase transition are believed to be crucial for the piezoelectric properties.

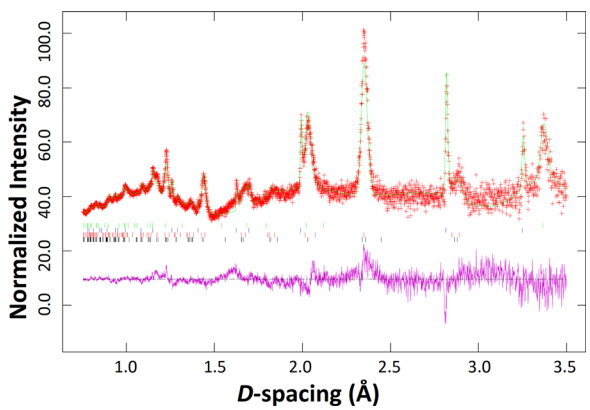

FIG. 8. Recovery run collected on a $Pb(Zr_{0.54}Ti_{0.46})O_3$ sample at 303 K and 0 GPa. Observed intensity is given by a red line and calculated intensity by a green line. The purple line gives the difference curve between measured and computed curves. The tick marks, from down to up, are from the $R3c$, Cm (due to the lower statistics of the recovery data constraints were introduced to the Cm phase so that true symmetry used in the refinements was $P4mm$), NaCl, and graphite phases. The rhombohedral phase fraction was 0.633(4).

IV. CONCLUSIONS

High-pressure neutron powder diffraction experiments were applied to the classical piezoelectric compound, $Pb(Zr_{0.54}Ti_{0.46})O_3$ up to 3 GPa and 773 K. This composition has two co-existing perovskite phases. Weight fraction changes between the rhombohedral *R*3*c* and monoclinic *Cm* (low-pressures and room temperature) or between *R*3*c* and tetragonal *P*4*mm* phases as a function of hydrostatic pressure and temperature were determined. The *Cm* phase was observed only at low-pressures and ambient temperatures as it continuously transformed to the *P*4*mm* phase at approximately 1 GPa and 400 K. As the earlier computations predicted, the rhombohedral phase was favored at higher pressures, whereas the added heat increased the tetragonal phase fraction at constant pressure. This largely contributes to the extrinsic piezoelectricity. These findings are in line with the computational model according to which the phase boundary between the rhombohedral and tetragonal phase in pressure-temperature plane is dictated by the two competing terms, octahedral tilting and entropy term. No support for a continuous polarization rotation was found. The oxygen octahedra was significantly distorted under pressure, accompanied by a significant displacement of the *B* cations. This contributes to the intrinsic piezoelectricity. After the experiments, the fraction of the *R*3*c* phase was larger than initially, suggesting that the *Cm* phase is not stable. This is consistent with the first-order phase transition $Cm \rightarrow R3c$. Irreversible changes are a continuous challenge for piezoelectric applications. We suggest a high-pressure sample synthesis technique for minimizing the *Cm* phase fraction in applications in which reversible performance is required.

ACKNOWLEDGMENTS

We would like to thank the reviewer for very carefully reading our manuscript and providing numerous constructive suggestions. The research work was supported by the collaboration project between the Center of Excellence for Advanced Materials Research at King Abdulaziz University in Saudi Arabia (Project No. T-001/431) and the Aalto University and the Academy of Finland (Projects 207071, 207501, 214131, and the Center of Excellence Program 2006-2011). This work has benefited from the use of the Lujan Neutron Scattering Center at Los Alamos Neutron Science Center, which is funded by the U.S. Department of Energy's Office of Basic Energy Sciences. Los Alamos National Laboratory is operated by Los Alamos National Security LLC under DOE Contract DE-AC52-06NA25396.

[1]B. Jaffe, W. R. Cook, and H. Jaffe, *Piezoelectric Ceramics* (Academic, New York 1971).
[2]H. Uwe, K. B. Lyons, H. L. Carter, and P. A. Fleury, Phys. Rev. B. **33**, 6436 (1986).
[3]E. Buixaderas, I. Gregora, S. Kamba, J. Petzelt, and M. Kosec, J. Phys.: Condens. Matter. **20**, 345229 (2008).
[4]J. Frantti and V. Lantto, Phys. Rev. B. **56**, 221 (1996).
[5]J. Frantti, V. Lantto, S. Nishio, and M. Kakihana, Phys. Rev. B. **59**, 12 (1999).
[6]C. M. Foster, Z. Li, M. Grimsditch, S.-K. Chan, and D. J. Lam, Phys. Rev. B. **48**, 10160 (1993).
[7]B. Noheda, D. E. Cox, G. Shirane, J. A. Gonzalo, L. E. Cross, and S.-E. Park, Appl. Phys. Lett. **74**, 2059 (1999).
[8]J. Frantti, J. Lappalainen, S. Eriksson, V. Lantto, S. Nishio, M. Kakihana, S. Ivanov, and H. Rundlöf, Jpn. J. Appl. Phys. Part 1 **39**, 5697 (2000).
[9]J. Frantti, S. Ivanov, S. Eriksson, H. Rundlöf, V. Lantto, J. Lappalainen, and M. Kakihana, Phys. Rev. B. **64**, 064108 (2002).
[10]R. E. Newnham, *Properties of Materials: Anisotropy, Symmetry, Structure* (Oxford University Press, New York, 2005).
[11]J. L. Jones, M. Hoffman, J. E. Daniels, and A. Studer, J. Appl. Phys. Lett. **89**, 092901 (2006).
[12]A. Pramanick, D. Damjanovic, J. C. Nino, and J. Jones, J. Am. Ceram. Soc. **92**, 2291 (2009).
[13]A. Pramanick, J. E. Daniels, and J. Jones, J. Am. Ceram. Soc. **92**, 2300 (2009).
[14]J. Y. Li, R. C. Rogan, E. Üstuñdag, and K. Bhattacharya, Nature Mater. **4**, 776 (2005).
[15]R. C. Rogan, E. Üstuñdag, B. Clausen, and M. R. Daymond, J. Appl. Phys. **93**, 4104 (2003).
[16]A. Grigoriev, R. Sichel, H. N. Lee, E. C. Landahl, B. Adams, E. M. Dufresne, and P. G. Evans, Phys. Rev. Lett. **100**, 027604 (2008).
[17]A. Grigoriev, R. J. Sichel, J. Y. Jo, S. Choudhury, L.-Q. Chen, H. N. Lee, E. C. Landahl, B. W. Adams, E. M. Dufresne, and P. G. Evans, Phys. Rev. B. **80**, 014110 (2009).
[18]J. Frantti, Y. Fujioka, and R. M. Nieminen, J. Phys. Chem. B. **111**, 4287 (2007).
[19]J. Frantti, Y. Fujioka, J. Zhang, S. C. Vogel, Y. Wang, Y. Zhao, and R. M. Nieminen, J. Phys. Chem. B. **113**, 7967 (2009).
[20]J. Frantti, Y. Fujioka, and R. M. Nieminen, J. Phys.: Condens. Matter. **20**, 472203 (2008).
[21]K. Momma and F. Izumi, "VESTA: A three-dimensional visualization system for electronic and structural analysis," J. Appl. Crystallogr. **41**, 653 (2008).
[22]N. W. Thomas and A. Beitollahi, Acta Crystallogr., Sect. B: Struct. Sci. **50**, 549 (1994).
[23]H. D. Megaw and C. N. W. Darlington, Acta Crystallogr., Sect. A: Cryst. Phys., Diffr., Theor. Gen. Crystallogr. **31**, 161 (1975).
[24]*International Tables for Crystallography A: Space-group Symmetry*, edited by Th. Hahn (Kluwer Academic, Dordrecht, 2005), pp. 804–808.
[25]J. Rouquette, J. Haines, V. Bornand, M. Pintard, Ph. Papet, W. G. Marshall, and S. Hull, Phys. Rev. B. **71**, 024112 (2005).
[26]J. Frantti, Phys. Chem. B. **112**, 6521 (2008).
[27]Y. Zhao, R. B. Von Dreele, and J. G. Morgan, High Press. Res. **16**, 161 (1999).
[28]Y. Zhao, D. He, J. Qian, C. Pantea, K. A. Lokshin, J. Zhang, and L. L. Daemen, "Development of high PT neutron diffraction at LANSCE—toroidal anvil press, TAP-98, in the HIPPO diffractometer," in *Advances in High-Pressure Technology for Geophysical Applications*, edited by J. Chen, Y. Wang, T. S. Duffy, G. Shen, and L. P. Dobrzhinetskaya (Elsevier Science & Technology, New York, 2005), pp. 461–474.
[29]H.-R. Wenk, L. Lutterotti, and S. Vogel, Nucl. Instrum. Methods Phys. Res. A **515**, 575 (2003).
[30]S. C. Vogel, C. Hartig, L. Lutterotti, R. B. Von Dreele, H.-R. Wenk, and D. J. Williams, Powder Diffr. **19**, 65 (2004).
[31]A. C. Larson and R. B. Von Dreele, *General Structure Analysis System* (LANSCE MS-H805, Los Alamos National Laboratory, Los Alamos, NM, 2000).
[32]B. H. Toby, J. Appl. Crystallogr. **34**, 210 (2001).
[33]D. L. Decker, J. Appl. Phys. **42**, 3239 (1971).
[34]J. Frantti, S. Eriksson, S. Hull, V. Lantto, H. Rundlöf, and M. Kakihana, J. Phys.: Condens. Matter. **15**, 6031 (2003).
[35]A. Sani, B. Noheda, I. A. Kornev, L. Bellaiche, P. Bouvier, and J. Kreisel, Phys. Rev. B. **69**, 020105 (2004).
[36]H. Yokota, N. Zhang, A. E. Taylor, P. Thomas, and A. M. Glazer, Phys. Rev. B. **80**, 104109 (2009).
[37]D. Phelan, X. Long, Y. Xie, Z.-G. Ye, A. M. Glazer, H. Yokota, P. A. Thomas, and P. M. Gehring, Phys. Rev. Lett. **105**, 207601 (2010).
[38]S. Gorfman, D. S. Keeble, A. M. Glazer, X. Long, Y. Xie, Z.-G. Ye, S. Collins, and P. A. Thomas, Phys. Rev. B. **84**, 020102 (2011).